



Influence of Sc³⁺ doping in B-site on electrochemical performance of Li₄Ti₅O₁₂ anode materials for lithium-ion battery



Yaoyao Zhang ^{a,1}, Chunming Zhang ^{b,*1}, Ye Lin ^c, Ding-Bang Xiong ^a, Dan Wang ^b, Xiaoyan Wu ^b, Dannong He ^{a,b,*}

^a School of Material Science and Engineering, Shanghai Jiao Tong University, No. 800 Dongchuan Road, Shanghai 200240, PR China

^b National Engineering Research Center for Nanotechnology, No. 28 East Jiangchuan Road, Shanghai 200241, PR China

^c Solid Oxide Fuel Cell SmartState Center, University of South Carolina, 541 Main Street, Columbia, SC 29208, USA

HIGHLIGHTS

- An enhanced chelating agent scheme for pure phase and uniformly distributed products.
- The bi-components chelating agent and Sc³⁺ doping to improve the particles dispersion and decrease the particle size.
- The Sc³⁺ doping could cause some Ti⁴⁺ reduce to Ti³⁺ and stimulate the formation of oxygen vacancies.
- Nano-scale Sc-doped Li₄Ti₅O₁₂ oxides show excellent reversible capacity and cycling stability.

ARTICLE INFO

Article history:

Received 12 September 2013

Received in revised form

26 October 2013

Accepted 30 October 2013

Available online 8 November 2013

Keywords:

Scandium doping
Sol–gel method
Lithium titanate
Anode material
Li-ion battery

ABSTRACT

Anode materials Li₄Ti₅O₁₂ (LTO) and Sc-doped Li₄Ti_{4.95}Sc_{0.05}O_{12-δ} (LTSO) for lithium-ion batteries are both successfully synthesized by the modified sol–gel method with ethylene diamine tetraacetic acid (EDTA) and citric acid (CA) as a bi-components chelating agent. The samples are characterized by XRD, BET, XPS, EDX and SEM. The dopant Sc totally enters into the 16d sites of the spinel structure of LTO, and then further affects its morphology and property. The LTSO powder exhibits a 3D network morphology and its grain size is about 200 nm. The LTSO electrode material exhibits an excellent initial discharge capacities of 174 and 94 mAh g⁻¹ at 1 C and 40 C, respectively. The reversible capacities of LTSO at different current rates remain nearly 100% after 50 cycles, which are compared with the capacities of the second cycles. Sc³⁺ doping can greatly improve the electronic conductivity of LTO which is demonstrated by electrochemical impedance spectroscopy. Cyclic voltammetry measurements also reveal that LTSO has small polarization resistance due to the high electrical conductivity and Li-ion apparent diffusion rate.

© 2013 Elsevier B.V. All rights reserved.

1. Introduction

In recent years, spinel Li₄Ti₅O₁₂ (LTO) oxide has been developed as a promising alternative anode material of lithium-ion batteries for large-scale application in electric vehicles and hybrid electric vehicles [1–4]. LTO anode shows a theoretical capacity of 175 mAh g⁻¹ within the voltage range of 1.0–3.0 V and an ultra-flat Li insertion voltage at ~1.55 V (vs. Li/Li⁺). Furthermore, it exhibits excellent Li-ion intercalation/extraction reversibility with near zero

volume change during the discharge/charge processes. Unfortunately, LTO shows relatively poor high rate capabilities because of a large polarization resistance due to the low electrical conductivity and Li-ion diffusion rate. Many approaches, including reducing the particle size [5,6], surface modification by oxides [7], metals [8–10] and carbon [11–14] coating and ion doping [15–19], have been introduced to improve the high rate performance of LTO anode.

Nowadays, ion doping is one of the most commonly used ways to alleviate the insulating property of LTO. Various ions have been doped into LTO structure, and then present remarkably different effects on the morphology and electrochemical property. Kubiak [20] once reported that partially replacing Ti by V, Mn and Fe could modify the cation distribution of crystallographic sites of LTO in 8a and 16d sites. Unfortunately, the dopant V, Mn and Fe elements have a negative influence on the electrochemical performances of LTO for two reasons: the defects of 16d sites reduce the capacity and

* Corresponding authors. National Engineering Research Center for Nanotechnology, No. 28 East Jiangchuan Road, Shanghai 200241, PR China. Tel.: +86 21 34291286; fax: +86 21 34291125.

E-mail addresses: zhangchm2003@163.com (C. Zhang), hdbill@sh163.net (D. He).

¹ These authors contributed equally to this work and share first authorship.

the defects of 8a sites create an irreversible insertion mechanism. Moreover, as reported by Sun [21], Cr ion can enter into the lattice structure in 16c sites owing to the similar ionic radius of Cr^{3+} to Ti^{4+} . The final result is the substitution of Cr ion reduces the area of special impedance and increases the rate capacity of LTO.

The synthesis method also has great impact on the properties of LTO. So far, LTO powders have been fabricated by several methods, including solid-state reaction method, sol–gel method, combustion synthesis method, hydrothermal method, and others [22–30]. Among these methods, the sol–gel synthetic route has been widely investigated due to its relatively less agglomeration of active materials through simple steps, and its products show excellent electrochemical performance simultaneously. In our previous work [31], LTO has been synthesized by a modified citric acid (CA) sol–gel method. Experiment results show a high capacity maintenance ratio of 97% after 1000 cycles at 1 C and 25 °C. However, its high rate discharge capacity is only 49 mAh g⁻¹ at 40 C. Thus, there may be still many opportunities, such as ion doping, for further improvement of the electrochemical performance of LTO.

As a new derived electrode material of solid oxide fuel cell, low concentration of Sc^{3+} doping in the B-site on $\text{La}_{0.8}\text{Sr}_{0.2}\text{MnO}_3$ [32] and $\text{SrCoO}_{3-\delta}$ [33] shows good structural, chemical stability and electrical conductivity under operation condition. Moreover, Sc is proved to introduce no Jahn–Teller distortion as there is no d orbital electron for Sc^{3+} (the electronic configuration of Sc^{3+} is $3s^23p^6$) [34]. When using Sc^{3+} as a dopant, Sc occupies part of 16d sites without changing the original structure of crystal. On the other side, the bond dissociation energy of $\text{Sc}–\text{O}$ is 674 kJ mol⁻¹ which is greater than that of $\text{Ti}–\text{O}$ (653 kJ mol⁻¹). Therefore, Sc^{3+} doping may greatly improve the performance of LTO electrode material for lithium-ion battery due to the changes of lattice parameters and bond energy. In the present work, nano-sized LTO and $\text{Li}_4\text{Ti}_{4.95}\text{Sc}_{0.05}\text{O}_{12-\delta}$ (LTSO) materials are prepared by the modified sol–gel route using ethylenediaminetetraacetic acid (EDTA) and CA as a bi-components chelating agent. The influence of Sc^{3+} doping in B-site on the lattice structure, particle size and the electrochemical properties of LTSO are investigated. The stability of the LTO without the Sc-doping is also studied by a half-cell system for comparison.

2. Experimental

2.1. Powder synthesis

LTSO was synthesized by the sol–gel method using the standard combined EDTA–CA as a chelating agent [35,36]. Tetrabutyl titanate (TBT), Li_2CO_3 and Sc_2O_3 (AR grade) were used as the raw materials. Stoichiometric amounts of Sc_2O_3 powder was first dissolved in HNO_3 and heated, and then TBT and Li_2CO_3 were dissolved in ethanol– HNO_3 preblended solution (the HNO_3 was used to inhibit the hydrolysis of TBT, the mole ratio of $\text{Li}:\text{Ti}:\text{Sc}$ is 4.2:4.95:0.05 and ethanol: HNO_3 is 50:1, solution A). The EDTA and CA were pre-dissolved in ammonia (the mole ratio of total metal ions to EDTA and to CA is 1:1:2, solution B). And the ammonia was aimed at rise the pH value of solution. Then the above solutions A&B were mixed, stirred and heated at 80 °C till the redundant solvent was evaporated. The resulting gelatin was heat-treated in an electric oven at 240 °C over 6 h to yield LTSO precursor. The solidified precursor was calcined under open air at 750 °C for 5 h to obtain final powders. The method, which yields the nano-sized LTSO material, was also applied to LTO preparation.

2.2. Electrode fabrication

The electrochemical cells consisted of cathode and anode plates which were separated by microporous polypropylene sheet and

electrolyte. The anode electrode was Li metal and the cathode electrode was $\text{Li}_4\text{Ti}_5\text{O}_{12}$ based composite which was prepared as follow steps. The LTSO powder, carbon electronic conductor (acetylene black) and polyvinylidene fluoride binder (PVDF) were mixed at a weight ratio of 85:10:5 in *N*-methyl-2-pyrrolidone (NMP) solvent. The slurry was then coated on the copper foil ($\sim 10 \mu\text{m}$) current collector and dried under vacuum at 120 °C for 12 h. The next step was to compress the composited electrode plate and then cut it to many small electrode plates of 12 mm diameter (the active material is about 1.8 mg). The electrolyte was 1 M solution of LiPF_6 in ethylene carbonate (EC) and dimethyl carbonate (DMC, EC:DMC = 1:1, v/v). Microporous polypropylene sheet (Celgard, 2400) was used as the separator. The cells were assembled in a glove box filled with pure argon.

2.3. Basic characterization

The crystal structures of the synthesized LTO and LTSO powders were examined by X-ray diffraction (XRD) using a Bruker D8 advance diffractometer with nickel filtered $\text{Cu K}\alpha$ radiation ($\lambda = 1.5418 \text{\AA}$, 45 kV, 50 mA, step size = 0.02°, $10^\circ \leq 2\theta \leq 80^\circ$). The surface chemical composition of the LTSO powder was monitored by X-ray photoelectron spectroscopy (XPS) measurements performed with a Kratos AXIS Ultra^{DLD} X-ray Photoelectron Spectrometer and a standard Al $\text{K}\alpha$ anode (1486.6 eV photon energy, 15 kV, 300 W). The particle morphology was observed using JEOL-6930 scanning electron microscopy (SEM). All the LTO and LTSO samples were painted on the aluminum foil. The specific surface area of the samples was determined by N_2 adsorption using a 3H-2000 specific surface area instrument (Brunauer–Emmett–Teller, BET).

2.4. Electrochemical characterization

The discharge/charge characteristics of the cells were performed over the potential range between 1.0 and 3.0 V using a NEWARE BTS 5 V–10 mA computer-controlled Galvanostat (Shenzhen, China) at different rates of 0.5–10 C at room temperature. Electrochemical impedance spectroscopy (EIS) was carried out using CHI660B electrochemical workstation (Shanghai Chenhua Instrument Co. Ltd., China) in the frequency range from 0.01 Hz to 1 MHz, which was in 3-electrode using metallic lithium film as the counter and reference electrode. Cyclic voltammetry tests were performed by a CHI660B electrochemical workstation over the potential range of 1.0–3.0 V versus Li^+/Li at the scanning rate of 0.5 mV s⁻¹.

3. Results and discussion

3.1. Powder characterization

The XRD patterns of the synthesized LTO samples with and without Sc^{3+} doping fired at different temperatures are shown in Fig. 1A. The precursor of LTSO shows an amorphous structure at the probe temperature below 400 °C. At 500 °C, the diffraction peaks corresponding to the intermediate phase of anatase TiO_2 , some impurity substances and spinel LTSO phase begin to appear. It also shows the intensity of the diffraction peaks of LTSO phase is gradually enhanced and the rutile TiO_2 phase sharply decreased with increasing the firing temperature more than 500 °C, which further indicates the crystallinity and grain size of LTSO are increasing with the increasing of the calcination temperatures. It can be seen that major diffraction peaks of LTSO and LTO matches very well and no new phase formation, which suggests that Sc^{3+} doping can not obviously change the spinel structure of LTO. In addition, as shown in Fig. 1B, it is observed that the diffraction peak (111) of LTSO slightly shifts to small angle, which should be

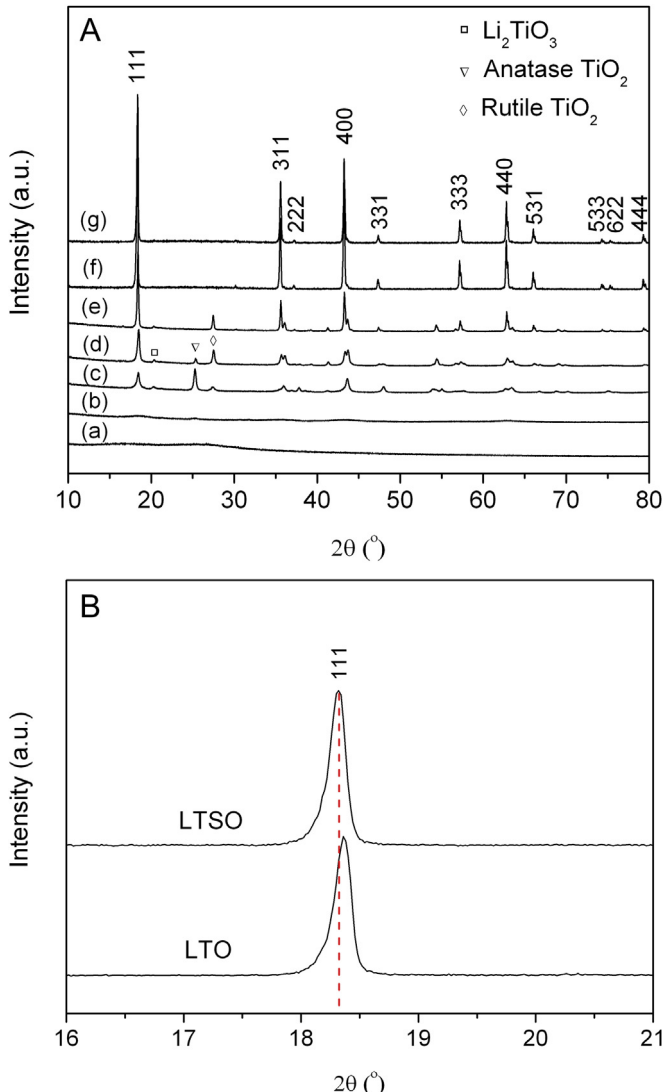


Fig. 1. X-ray diffraction patterns of LTSO precursor dried at 240 °C (a) and then calcined at 400 °C (b), 500 °C (c), 600 °C (d), 700 °C (e), 750 °C (f) and LTO sample calcined at 750 °C (g) for 5 h (A) and the partial enlarged drawing of (111) diffraction peak (B).

attributed to the replacement of some Ti^{4+} for Sc^{3+} in B sites and to the fact that the ionic size of the Sc^{3+} (0.075 nm) is larger than that of Ti^{4+} (0.061 nm). It may be preliminarily concluded that the dopant Sc has entered into the lattice structure of LTSO which has excellent crystallinity. However, one of the most remarkable things is that the content of Sc element is far less than 5 wt% in LTSO sample, which is calculated by stoichiometric. The electronic state of Sc and Ti elements that exist with LTSO material need to be further proved by XPS.

Fig. 2A shows XPS spectra of LTO and LTSO samples tested under the same conditions. Photoelectron peaks of O, Ti and C elements were clearly observed on the surface of LTO and LTSO powders. It is well known that the carbon element in Fig. 2A is likely to come from carbon contamination inside XPS instruments. However, the position of the C 1s peak can be used for calibration. The binding energies used in quantitative measurements are shown as follows: C 1s at 285 eV, Li 1s at 55 eV, Ti 2p at 457 eV, Sc 2p at 402 eV and O 1s at 530 eV. As shown in Fig. 2A & B, very weak signals for Sc 2p were detected for LTSO due to the very low ion doping content. Based on the Handbooks of Monochromatic XPS Spectra (DEMO

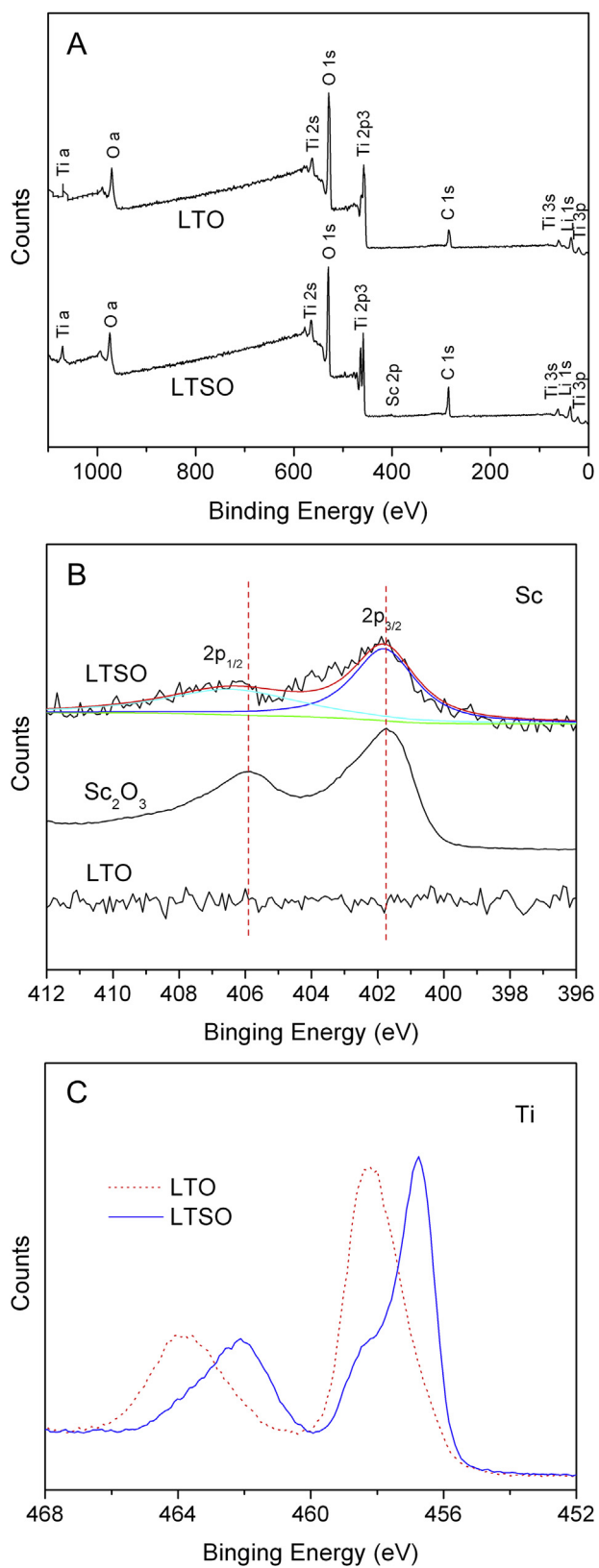


Fig. 2. XPS survey spectra (A) and high resolution XPS spectra of Sc 2p (B) and Ti 2p (C) measured from Sc_2O_3 , LTO and LTSO powder.

Version, B.V. Crist, 1999), the position of the Sc 2p_{3/2} peak is around 401.9 eV and the valance state of Sc is +3. As shown in Fig. 2B, the two peaks of Sc 2p_{3/2} in LTSO and Sc₂O₃ were both identified at around 401.9 eV. There was a binding energy difference of about 0 eV between the Sc 2p_{3/2} peaks of Sc₂O₃ and LTSO in this study. Hence, these observations indicate that Sc ions are in the state of +3 in LTSO. Meanwhile the two peaks of Sc 2p_{1/2} in LTSO and Sc₂O₃ were identified at 406.9 eV and 405.9 eV, respectively. There was a binding energy difference of about 1 eV between the Sc 2p_{1/2} peaks of Sc₂O₃ and LTSO. Some changes, i.e. peak width, peak shape and peak position, between Sc₂O₃ and LTSO in Fig. 2B were also observed, which could be attributed to the Sc³⁺ doping in B-site of LTO on its lattice structure. In addition, compared with the XPS spectrum of Ti 2p_{3/2} and Ti 2p_{1/2} of LTO, a very slight shift can be observed in LTSO powder (as shown in Fig. 2C), indicating the Ti³⁺ detection is on the outer surface. Furthermore, lattice parameters of LTO and LTSO were calculated to be 8.358 and 8.359 Å based on the normal spinel space group of $Fd\bar{3}m$, respectively. Therefore, the Sc³⁺ has been successfully doped into the lattice structure of LTO and then some Ti³⁺ has been produced on the surface of LTSO.

Fig. 3A & B shows the SEM images of the LTO samples with and without Sc³⁺ doping. It is obvious that both samples exhibit a uniform distribution of three-dimensional space network structure, and the particle sizes are 200–500 nm and 100–300 nm, respectively. Combined with the results of the BET surface area, it can be seen that the particle size of LTO sample actually decreases after the Sc³⁺ doping. As shown in Fig. 3C & D, energy dispersive X-ray spectroscopy (EDX) has been done to identify the distribution of Ti and Sc in LTSO. It suggests that both Ti and Sc are uniformly distributed in the crystal lattice of LTSO. Furthermore, a much higher BET surface area of LTSO than LTO at the same calcination temperature was observed, which should be ascribed to the

excessive amount of HNO₃ added for dissolving Sc₂O₃ in the synthesis of LTSO powder. Referring to our previous research, the sintering temperatures of 750 °C for LTO (BET surface area ~4.34 m² g⁻¹) and LTSO (BET surface area ~7.42 m² g⁻¹) were chosen to obtain powders with good crystallinity for further tests. To further detect whether exist Sc in the surface of LTO, significant Sc formation was supported by the EDX detection as shown in Fig. 4. It is well known that the EDX is not an ideal tool for the detection of carbon and oxygen contents due to the easy carbon and oxygen contamination during the sample preparation process, especially for quantitatively determination of the content. Therefore, we only verify whether the ratio of Ti:Sc elements could be in line with the stoichiometric ratio. As shown in Fig. 4A and Table 1, the average ratio of Ti:Sc for five different point area was around 99 (the stoichiometric ratio of Ti:Sc = 99:1). It further demonstrates that the dopant Sc has totally entered into the lattice structure of LTSO.

As for the spinel structure of pristine LTO, three fourths of Li⁺ ions occupy the tetrahedral 8a sites, the rest of Li⁺ ions and Ti⁴⁺ ions occupy the 1/6 and 5/6 of 16d sites, respectively. The 32e sites are occupied by the oxygen atoms [37–40]. Expressing the above distribution in LTO structure, the stoichiometry can be written as [Li]_{8a}[Li_{1/3}Ti_{5/3}]_{16d}[O₄]_{32e}. However, the 16c sites are structurally vacant. During the discharge process, the enthetic Li⁺ ion insert into the vacant 16c sites and the internal Li⁺ ions in 8a sites transfer into 16c sites at the same time. Hence, the 8a sites turn empty. So the discharge process of LTO can also be described as the phase transition from spinel structure ([Li]_{8a}[Li_{1/3}Ti_{5/3}]_{16d}[O₄]_{32e}) to rock-salt structure ([Li₂]_{16c}[Li_{1/3}Ti_{5/3}]_{16d}[O₄]_{32e}). It is well known that the valence-state change of Ti ion from 4+ to 3+ or the existence of oxygen vacancy due to the ion doping has been mentioned in many literature [6,15,16,41,42]. Here, the Sc-doping will change the

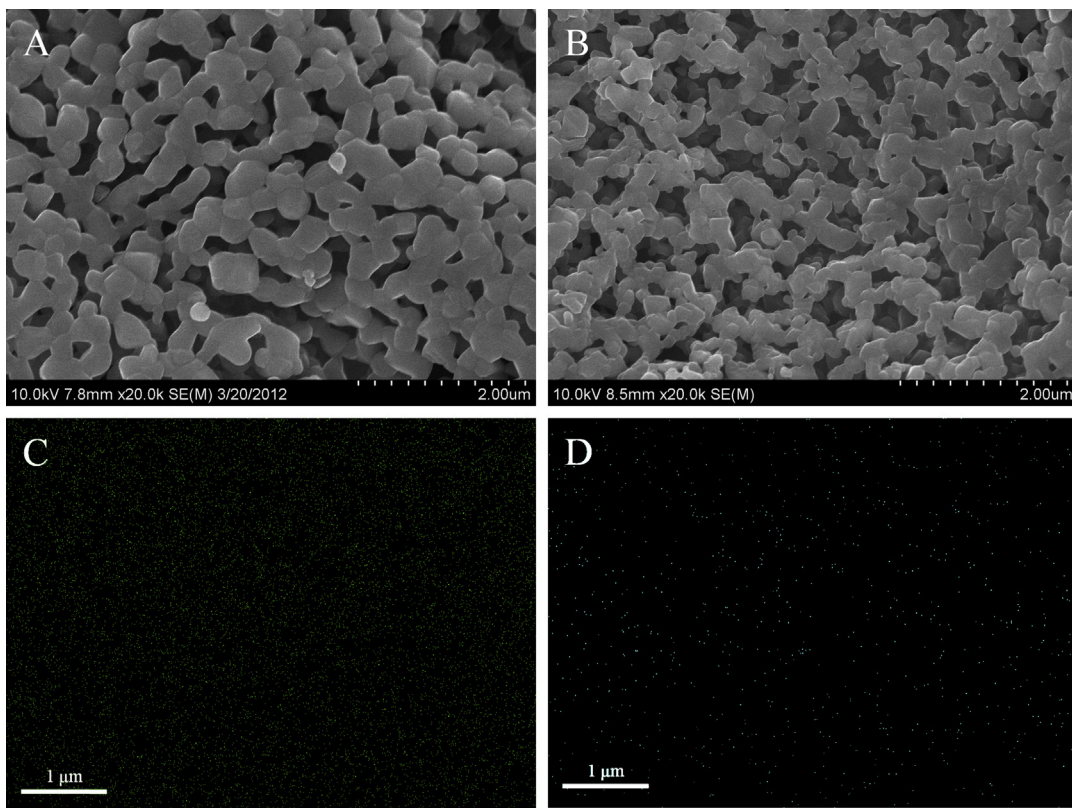


Fig. 3. SEM images of the obtained LTO (A) and LTSO (B) powders; and the EDX element mapping of Ti (C) and Sc (D) on the LTSO particles.

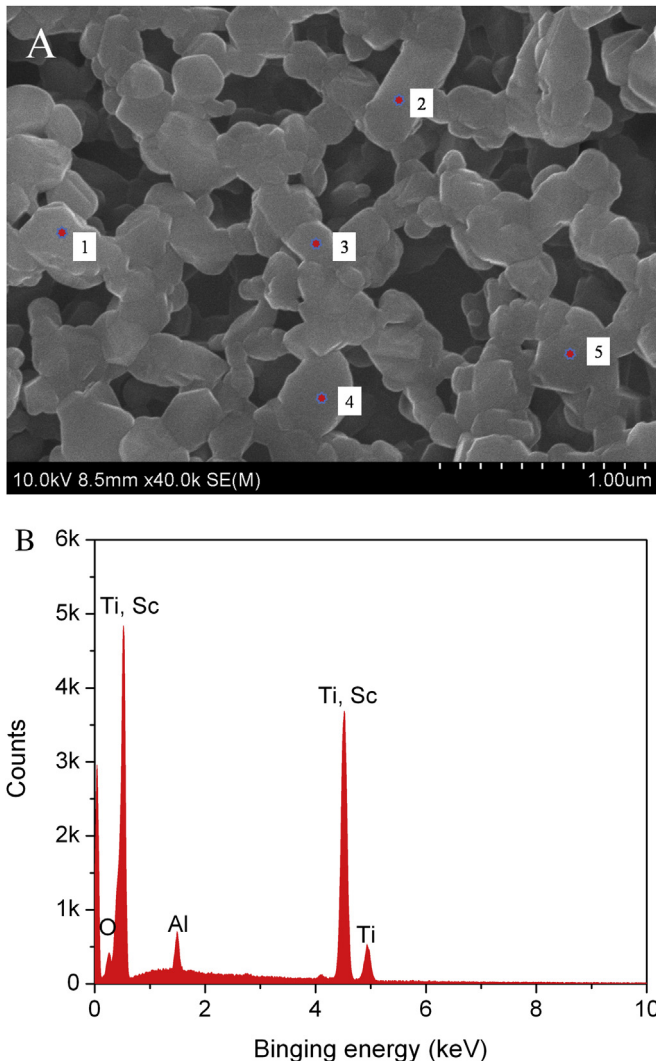


Fig. 4. SEM image of the pristine LTSO powder at high magnification (A) and the related EDX analysis of LTSO at point area 1(B).

occupancy situation of spinel structure of LTO where the 16d sites may be partially occupied by Sc^{3+} ions. In order to further investigate the structure of LTSO and the influence of Sc^{3+} doping, a structure model has been made according to the neutron diffraction data which has been reported by Aldon [37]. As shown in Fig. 5, the Sc^{3+} doping could cause some Ti^{4+} reduce to Ti^{3+} within the octahedron coordinated framework. And then the oxygen vacancies and the deformation of polyhedron may be present in LTSO structure. The doping of Sc^{3+} on Ti^{4+} site and oxygen vacancies will cause the transition of a small quantity of Ti ions from Ti^{4+} to Ti^{3+} as charge compensation. Therefore, the number of electrons was increased and hence, electronic conductivity. As a result, it is believed that the Sc^{3+} ions into the spinel structure of LTO will further improve its electrochemical performance.

3.2. Electrochemical characterization

The grain size and morphology of the active materials in Li-ion battery typically have a significant effect on their electrochemical performance. A larger specific surface area means more active sites in electrode materials, and thus a higher first discharge/charge capacities will be observed. In order to enable active the real

Table 1
EDX data of LTSO by spot scan method in Fig. 4A's different areas.

Number	Sc (mass percent, %)	Ti (mass percent, %)	Ti:Sc (mole ratio)
1	0.37	37.59	95.42
2	0.42	44.32	99.11
3	0.33	35.47	100.95
4	0.29	31.35	101.53
5	0.36	39.25	102.40
Average	—	39.88	99.88

capacity of the electrode material, the cell was discharged and charged under 0.5 C rate for two cycles before testing. Fig. 6A shows the discharge/charge curves of the cell with the LTSO electrode at the rate between 1 C and 40 C over the voltage range between 1.0 and 3.0 V. It clearly shows that the first discharge capacities reached 174, 171, 161, 143, 121 and 94 mAh g^{-1} corresponding to the discharge rates of 1 C, 2 C, 5 C, 10 C, 20 C and 40 C, respectively. The capacities gradually drop by the increasing of discharge/charge rate. As shown in Table 2 and Fig. 6B, the obtained first specific discharge capacity of LTSO is higher than that reported by Wang et al. [43] for LTO and $\text{Li}_{3.95}\text{La}_{0.05}\text{Ti}_5\text{O}_{12}$ (La–LTO). Moreover, compared with other doped LTO electrode materials in literature [42,44–48], it still possess much better high-rate performance. Fig. 6B shows the cycling performance of LTO and LTSO at the rate between 1 C and 40 C. It can be seen that Sc-doped LTO shows the great superiority on specific capacities at high rates, meanwhile, the difference between the capacities of LTO and LTSO increases with the increasing of the current rates. This improvement of the high rate capacities of LTSO could be related to the improved specific surface area and the Li ion extraction/insertion and electronic apparent diffusion rate. Fig. 6B also shows the discharge capacities of LTSO at 1 C, 2 C and 5 C rates are exceptionally stable with the increasing number of cyclings. However, there are some capacity losses appeared at the early few cycles at high discharge/charge rates between 10 C and 40 C. This could be attributed to the Li insertion into the LTO's bulk phase can't completely deintercalated from 16c sites when charge rate is suddenly changed from low rates to high rates or the possible decomposition of the organic electrolyte [31]. Therefore, further work about the electrode kinetics needs to be done.

The cycling behavior of the same cell at the discharge/charge rate range between 1 C and 40 C within a potential range between 1.0 and 3.0 V was further carried out, which was progressively discharged and charged for 50 cycles in series stages. As shown in Fig. 7, the relatively stable discharged capacities were observed at all stages. After the initial capacity loss, all the curves show smooth horizontal lines and very high capacity retentions upon cycling. As can be seen from Table 3 that all the capacity retentions are more than 90%, and the capacity of Sc-doped LTO was 167 and 77 mAh g^{-1} at 1 C and 40 C rates after 50 cycles, respectively. Compared to our previous work [31], the capacities of pristine LTO material are only 162 and 41 mAh g^{-1} at the same operation conditions. These results suggest that the Sc^{3+} doping in B-site of LTO is very effective in enhancing the electrochemical performance especially at high rate capacity. Furthermore, it is very interesting that if we ignore the first cycle, the capacity retention could exceed 99%. Hence, according to the results obtained in this work, the nano-LTSO is considered to be an excellent electrode material.

Fig. 8A and B shows the Nyquist plots and equivalent circuit of the LTO electrode with and without Sc^{3+} doping in the frequency range of 100 kHz to 0.01 Hz. The experimental results could be fitted well with the proposed equivalent circuit. In the equivalent circuit, R_s is attributed to the ohmic resistance of the electrolyte; R_{ct} indicates the charge transfer resistance at the active material interface; R_f is the polarization resistance; C_{dl} represents the

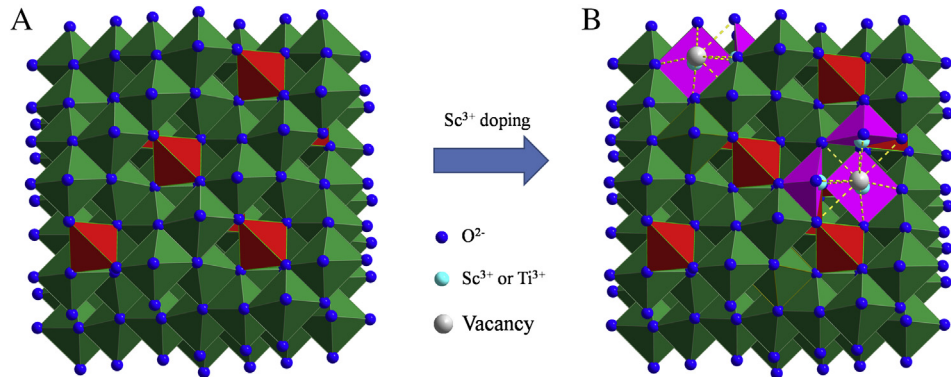


Fig. 5. Lattice structure image of LTO (A) and LTSO (B) which is the view along the (110) direction, correspond to the 8a, 16d and 32e sites. The centers of red tetrahedra and green octahedra are lithium (8a) and lithium/titanium (16d). The light red polyhedron distortion is the result of Sc³⁺ doping or Ti⁴⁺ reduced to Ti³⁺. (For interpretation of the references to color in this figure legend, the reader is referred to the web version of this article.)

double-layer capacitance, and C_f is the surface capacitance. Z_w means the Warburg impedance caused by a semi-infinite diffusion of Li⁺ in the electrode. After going through the simulation, the R_{ct} for the LTSO electrode ($R_{ct} = 66 \Omega$) is much smaller than the

undoped LTO ($R_{ct} = 72 \Omega$). This result indicates that the charge transfer at the electrolyte/electrode interface is greatly improved after Sc³⁺ doping. Based on the relationship between the real axis Z' and the reciprocal square root of the lower angular frequencies $\omega^{-0.5}$, the Warburg impedance coefficient σ_w can be obtained from Fig. 9, and then the Li-ion diffusion coefficient D can be calculated. The chemical diffusion coefficient of Li⁺ can be estimated according to the Fick's law [49,50].

$$D = \frac{R^2 T^2}{2A^2 n^4 F^4 C^2 \sigma_w^2}$$

Here, D is the diffusion coefficient of lithium ion, R is the gas constant, T is the absolute temperature, A is the surface area of the electrode, n is the number of electrons per molecule during oxidation, F is the Faraday constant, C is the concentration of lithium ion, and σ_w is the Warburg factor. The conductivity measurement shows the value of D is $9.13 \times 10^{-12} \text{ cm}^2 \text{ s}^{-1}$ and $5.16 \times 10^{-14} \text{ cm}^2 \text{ s}^{-1}$ for the LTO with and without Sc³⁺ doping, respectively. Based on the above results, the Sc³⁺ doping into LTO significantly improve the Li⁺ apparent diffusion rate and reduce the charge transfer resistance which exhibits much better electrochemical performance compared with the undoped LTO electrode.

Fig. 10 shows the cyclic voltammograms of cells using LTO and LTSO as active materials at the scanning rate of 0.5 mV s^{-1} between 1.0 and 3.0 V. As shown in Fig. 8, the cyclic voltammogram curves of LTO and LTSO are similar. There is only one pair of reduction and oxidation peak appearing on the cyclic voltammogram curve of LTSO and the redox peaks are extremely sharp and well-defined splitting. That means Sc-doped LTO are well crystallized and pure, which is in accordance with the result of XRD examination. Furthermore, the cathodic peak corresponding to the voltage platform of the first discharge process in which Li intercalated into the LTSO anode is located at $\sim 1.52 \text{ V}$ (vs. Li) and the anodic peak

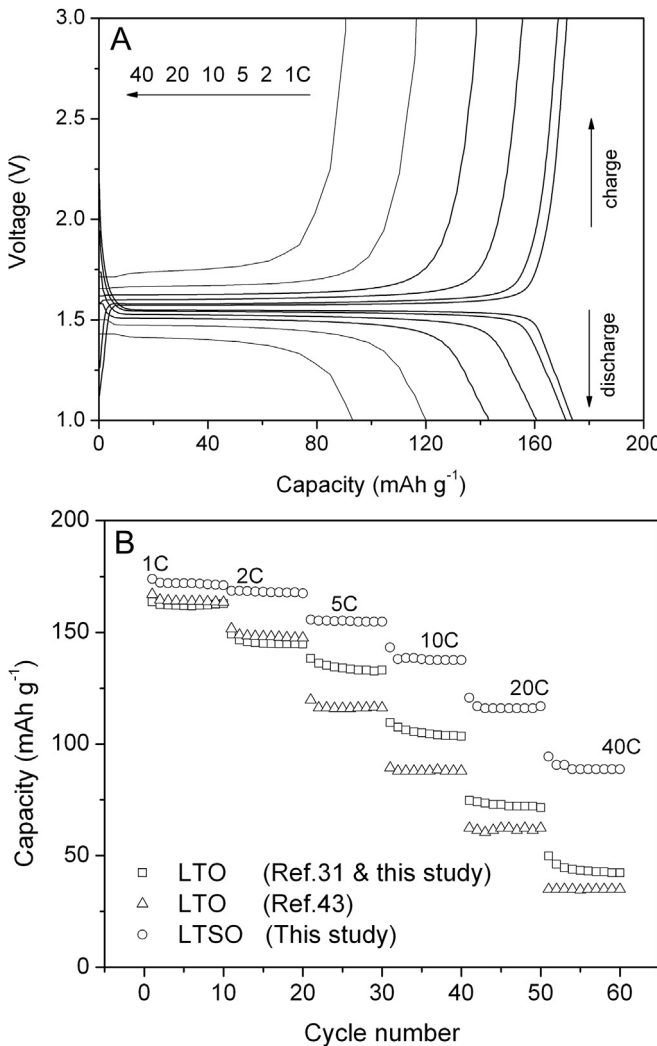


Fig. 6. The first discharge–charge curves of LTSO (A) and five cycling performance of LTSO and LTO produced by modified sol–gel method and LTO produced by solid state method in our previous work (B) at the discharge rate range between 1 C and 40 C within a potential range between 1.0 and 3.0 V.

Table 2

The first discharge capacities of electrode materials prepared by the EDTA-CA sol–gel method (Ref. [31] and this study) and solid-state reaction method (Ref. [43]) at the discharge/charge rate range between 1 C and 40 C.

Rate	The first discharge capacity (mAh g ⁻¹)			
	LTSO	LTO (Ref. [31])	LTO (Ref. [43])	La–LTO (Ref. [43])
1 C	174	164	167	171
2 C	171	149	152	161
5 C	161	138	120	139
10 C	143	110	89	112
20 C	121	75	62	82
40 C	94	50	35	55

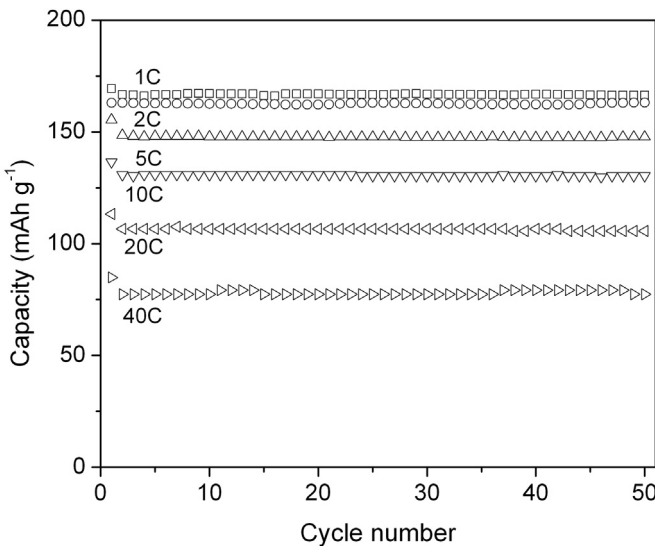


Fig. 7. The cyclic performance of LTSO at the discharge rate range between 1 C and 40 C within a potential range between 1.0 and 3.0 V.

Table 3
Capacity retention of LTSO prepared by the EDTA-CA sol-gel method at the discharge/charge rate range between 1 C and 40 C after 50 cycles.

Rate	Capacity at different cycles (mAh g ⁻¹)			Capacity retention (%)	
	1st (C ₁)	2nd (C ₂)	50th (C ₅₀)	C ₅₀ /C ₁	C ₅₀ /C ₂
1 C	169	167	167	98.8	100
2 C	163	163	163	100	100
5 C	155	149	148	95.5	99.3
10 C	137	131	130	94.9	99.2
20 C	113	107	106	93.8	99.1
40 C	85	77	77	90.6	100

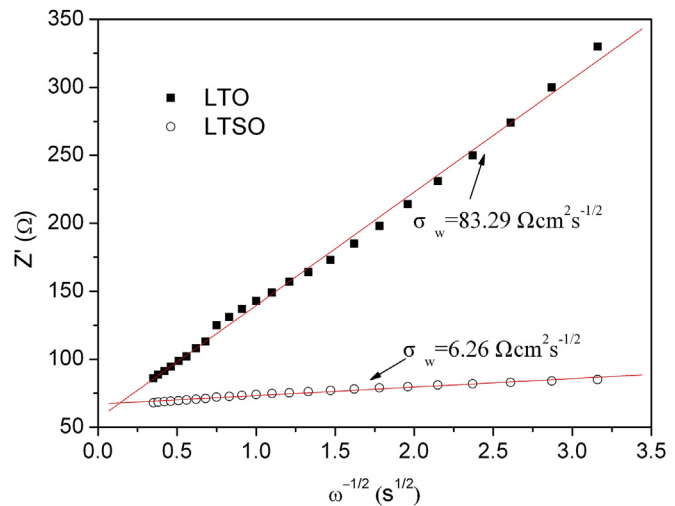


Fig. 9. The relationship between real impedance with the low frequencies of the LTO half cell with and without the Sc³⁺ doping in the original state.

corresponding to the voltage platform of the first charge process in which Li deintercalated from the anode is located at ~1.65 V (vs. Li). For pristine LTO, the cathodic peak and anodic peak is located at ~1.51 V and ~1.65 V, respectively. The potential difference between the first anodic and cathodic peaks was reduced from 140 mV to 130 mV. Such differences may be caused by the influence of particle size and inherent properties of electrode materials on the electrochemical performance. As a result, the electrode polarization of LTSO is not as serious as that of LTO and therefore LTSO is supposed to get better electrochemical performances at high discharge current rates which is well confirmed by the result of Fig. 6.

4. Conclusions

Nano-scale LTO and Sc-doped LTO materials have been successfully synthesized by EDTA-CA sol-gel method. The products calcined at 750 °C for 5 h show very pure phase and uniform particle size distribution. The dopant Sc has totally entered into the B site of the lattice structure of LTO. The LTSO sample has smaller particle size and higher specific surface area than the undoped LTO. The electrochemical performance of LTSO exhibits excellent

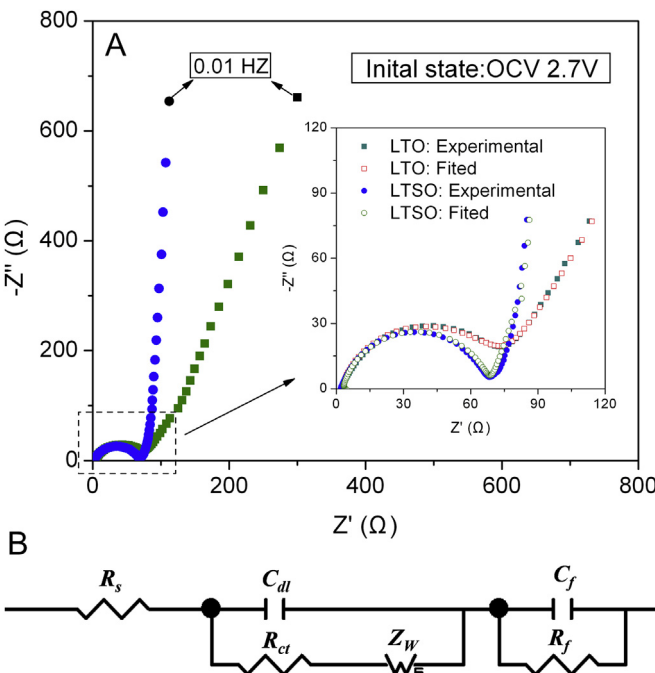


Fig. 8. Electrochemical impedance spectra of the LTO half cell with and without the Sc³⁺ doping at the original state (A) and related equivalent circuit (B).

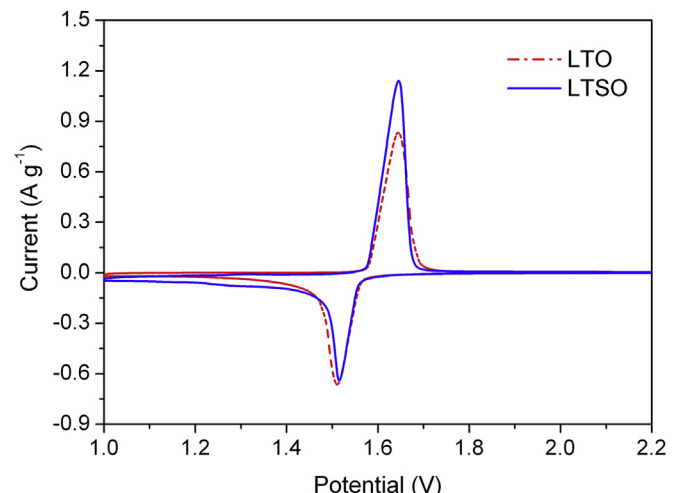


Fig. 10. Cyclic voltammograms of cells using LTO and LTSO as anode materials at the scanning rate of 0.5 mV s⁻¹.

discharge capacities of 174 and 94 mAh g⁻¹ at 1 C and 40 C discharge rate, respectively. Sc³⁺ substitution greatly increased the reversible capacity and cycling stability of LTO at low discharge rates. Furthermore, LTSO has been proved to have smaller charge transfer resistance and higher lithium-ion diffusivity by EIS measurements. All the results demonstrate that Sc³⁺ doping is beneficial to the reversible intercalation and extraction of Li ion. Thus, the LTSO is a very promising high rate electrode material for lithium-ion batteries.

Acknowledgments

This work was supported by the National Natural Science Foundation of China under contract No. 21171116 and the International Science & Technology Cooperation Program of China under contract No. 2012DFG11660. The first author would also like to thank Pro. Jun Yang at Shanghai Jiao Tong University for offering help with some discussions.

References

- [1] J.B. Goodenough, Y. Kim, *Chem. Mater.* 22 (2010) 587–603.
- [2] M. Armand, J.M. Tarascon, *Nature* 451 (2008) 652–657.
- [3] C. Samaras, K. Meisterling, *Environ. Sci. Technol.* 42 (2008) 3170–3176.
- [4] H.G. Jung, M.W. Jang, J. Hassoun, Y.K. Sun, B. Scrosati, *Nat. Commun.* 2 (2011) 516–520.
- [5] G. Wang, J. Xu, M. Wen, R. Cai, R. Ran, Z. Shao, *Solid State Ionics* 179 (2008) 946–950.
- [6] W.J.H. Borghols, M. Wagemaker, U. Lafont, E.M. Kelder, F.M. Mulder, *J. Am. Chem. Soc.* 131 (2009) 17786–17792.
- [7] S. Huang, Z. Wen, X. Zhu, X. Yang, *J. Electrochem. Soc.* 152 (2005) A1301–A1305.
- [8] A. Sivashanmugam, S. Gopukumar, R. Thirunakaran, C. Nithya, S. Prema, *Mater. Res. Bull.* 46 (2011) 492–500.
- [9] C. Li, Q. Li, L. Chen, T. Wang, *ACS Appl. Mater. Interface* 4 (2012) 1233–1238.
- [10] J.G. Kim, D. Shi, M.S. Park, G. Jeong, Y.U. Heo, M. Seo, Y.J. Kim, J.H. Kim, S.X. Dou, *Nano Res.* 6 (2013) 365–372.
- [11] Y. Wang, H. Liu, K. Wang, H. Eiji, Y. Wang, H. Zhou, *J. Mater. Chem.* 19 (2009) 6789–6795.
- [12] Z. Wang, G. Xie, L. Gao, *J. Nanomater.* 2012 (2012) 1–7.
- [13] T. Yuan, X. Yu, R. Cai, Y. Zhou, Z. Shao, *J. Power Sources* 195 (2010) 4997–5004.
- [14] G. Zhu, H. Liu, J. Zhuang, C. Wang, Y. Wang, Y. Xia, *Environ. Sci. Technol.* 4 (2011) 4016–4022.
- [15] J. Wolfenstine, J.L. Allen, *J. Power Sources* 180 (2008) 582–585.
- [16] Y. Qi, Y. Huang, D. Jia, S. Bao, Z.P. Guo, *Electrochim. Acta* 54 (2009) 4772–4776.
- [17] H. Pan, L. Zhao, Y.S. Hu, H. Li, L. Chen, *ChemSusChem* 5 (2012) 526–529.
- [18] L. Zhao, Y. Hu, H. Li, Z. Wang, L. Chen, *Adv. Mater.* 23 (2011) 1385–1388.
- [19] N. Li, G. Zhou, F. Li, L. Wen, H.M. Cheng, *Adv. Funct. Mater.* (2013), <http://dx.doi.org/10.1002/adfm.201300495>.
- [20] P. Kubiaik, A. Garcia, M. Wormes, L. Aldon, J. Olivier Fourcade, P.E. Lippens, J.C. Jumas, *J. Power Sources* 119–121 (2003) 626–630.
- [21] Y.K. Sun, D.J. Jung, Y.S. Lee, K.S. Nahm, *J. Power Sources* 125 (2004) 242–245.
- [22] Y.Q. Xu, G.C. Liang, L. Wang, *Adv. Mater. Res.* 347–353 (2011) 3439–3442.
- [23] E. Kang, Y.S. Jung, G.H. Kim, J. Chun, U. Wiesner, A.C. Dillon, J.K. Kim, J. Lee, *Adv. Funct. Mater.* 21 (2011) 4349–4357.
- [24] L. Shen, E. Uchaker, X. Zhang, G. Cao, *Adv. Mater.* 24 (2012) 6502–6506.
- [25] M. Ganeshan, M.V.T. Dhananjeyan, K.B. Sarangapani, N.G. Renganathan, *J. Electroceram.* 18 (2007) 329–337.
- [26] N.A. Alias, M.Z. Kufian, L.P. Teo, S.R. Majid, A.K. Arof, *J. Alloys Compd.* 486 (2009) 645–648.
- [27] T. Yuan, K. Wang, R. Cai, R. Ran, Z. Shao, *J. Alloys Compd.* 477 (2009) 665–672.
- [28] T.F. Yi, Y. Xie, Q. Wu, H. Liu, L. Jiang, M. Ye, R. Zhu, *J. Power Sources* 214 (2012) 220–226.
- [29] L. Yu, H.B. Wu, X.W. Lou, *Adv. Mater.* 25 (2013) 2296–2300.
- [30] C. Kim, N.S. Norberg, C.T. Alexander, R. Kostecki, J. Cabana, *Adv. Funct. Mater.* 23 (2013) 1214–1222.
- [31] C. Zhang, Y. Zhang, J. Wang, D. Wang, D. He, Y. Xia, *J. Power Sources* 236 (2013) 118–125.
- [32] H. Gu, Y. Zheng, R. Ran, Z. Shao, W. Jin, N. Xu, J. Ahn, *J. Power Sources* 183 (2008) 471–478.
- [33] P. Zeng, R. Ran, Z. Chen, H. Gu, Z. Shao, S. Liu, *AIChE J.* 53 (2007) 3116–3124.
- [34] F. Zhou, X. Zhao, H. Zheng, Z. Zhang, M. Ji, *Mater. Lett.* 58 (2004) 3720–3724.
- [35] C. Zhang, Y. Zheng, Y. Lin, R. Ran, Z. Shao, D. Farrusseng, *J. Power Sources* 191 (2009) 225–232.
- [36] W. Zhou, Z. Shao, W. Jin, *J. Alloys Compd.* 426 (2006) 368–374.
- [37] L. Aldon, P. Kubiaik, M. Wormes, J.C. Jumas, J. Olivier-Fourcade, J.L. Tirado, J.I. Corredor, C.P. Vicente, *Chem. Mater.* 16 (2004) 5721–5725.
- [38] E.M. Sorensen, S.J. Barry, H.K. Jung, J.R. Rondinelli, J.T. Vaughey, K.R. Poeppelmeier, *Chem. Mater.* 18 (2006) 482–489.
- [39] J. Haetge, P. Hartmann, K. Brezesinski, J. Janek, T. Brezesinski, *Chem. Mater.* 23 (2011) 4384–4393.
- [40] A.S. Prakash, P. Manikandan, K. Ramesha, M. Sathiya, J.M. Tarascon, A.K. Shukla, *Chem. Mater.* 22 (2010) 2857–2863.
- [41] Y.M. Chiang, D. Birnie III, W.D. Kingery, *Physical Ceramics*, Wiley, New York, 1997.
- [42] C.H. Chen, J.T. Vaughey, A.N. Jansen, D.W. Dees, A.J. Kahalan, T. Goacher, M.M. Thackeray, *J. Electrochem. Soc.* 148 (2001) A102–A104.
- [43] D. Wang, C. Zhang, Y. Zhang, J. Wang, D. He, *Ceram. Int.* 39 (2013) 5145–5149.
- [44] C. Qiu, Z. Yuan, L. Liu, N. Ye, J. Liu, *J. Solid State Electrochem.* 17 (2012) 841–847.
- [45] H. Li, L. Shen, X. Zhang, P. Nie, L. Chen, K. Xu, *J. Electrochem. Soc.* 159 (2012) A426–A430.
- [46] B. Zhang, Z. Huang, S.W. Oh, J.K. Kim, *J. Power Sources* 196 (2011) 10692–10697.
- [47] W. Long, X. Wang, S. Yang, H. Shu, Q. Wu, Y. Bai, L. Bai, *Mater. Chem. Phys.* 131 (2011) 431–435.
- [48] S. Huang, Z. Wen, X. Zhu, Z. Lin, *J. Electrochem. Soc.* 152 (2005) A186–A190.
- [49] C. Ho, I.D. Raistrick, R.A. Huggins, *J. Electrochem. Soc.* 127 (1980) 343–350.
- [50] B. Li, C. Han, Y.B. He, C. Yang, H. Du, Q.H. Yang, F. Kang, *Energy Environ. Sci.* 5 (2012) 9595–9602.